Customization of 3D-Printed Hinged Ankle-Foot Orthosis Based on Kinematic Evaluation from Motion Capture

Customization of 3D-printed hinged ankle-foot orthosis based on kinematic evaluation from motion capture

Carlo De Benedictis *[0000-0003-0687-0739], Maria Paterna [0000-0001-5484-7491], Alessia Dipalma, Martina Piazzolla, Daniela Maffiodo [0000-0002-5831-8156], Walter Franco [0000-0002-0783-6308], Carlo Ferraresi [0000-0002-9703-9395]

Department of Mechanical and Aerospace Engineering, Politecnico di Torino, Turin, Italy
carlo.debenedictis@polito.it

Abstract. Commercial hinged foot-ankle orthoses (HAFO) generally do not ensure the alignment between the mechanical and the anatomical joints, causing discomfort and unnatural walking. This paper presents a method to design a customized HAFO modeled on geometrical and kinematic data collected from a healthy 24-year-old woman. The geometry of the shank and foot was acquired through a 3D scanner. The physiological articular rotation axis (AoR) was estimated through helical axis and SARA algorithms. The identified AoR was then used to properly design the orthosis by making particular attention to the hinge position. Finally, the prototype was manufactured with fused deposition modeling technique, and its functionality was validated through gait analysis trials.

Keywords: Hinged ankle-foot orthoses, Joint axis of rotation, 3D-printed orthotics, Custom-made orthoses, Orthosis design.

1 Introduction

Ankle-foot orthoses (AFO) are used to completely or partially restrict ankle joint motion [1]. Depending on their functionality and architecture, AFO can be classified into: solid AFO (SAFO) [2]; dynamic AFO (DAFO) [3], posterior leaf spring AFO (PLS AFO) [4]; hinged AFO (HAFO) [5]. The latter are made up of two shells, one on the foot and the other on the shank, joined by a mechanical hinge that permits some relative movement between these two segments, especially in the sagittal plane. It has been proven that HAFO can appropriately support this motion in actual patients, especially when it comes to returning to normal function. Yet, the design of these devices must carefully consider where to locate the mechanical hinge between the two shells. If not correctly designed and positioned, HAFO can contribute to unnatural gait [6].

To assess ankle joint's axis of rotation (AoR), numerical methods have been developed in support of experimental analyses that can be conducted in-vivo and in-vitro [7–10]. Contrary to predictive strategies, functional methods for joint kinematics assessment do not rely on regression equations or particular marker positioning protocols. In such approaches, it is still necessary to track the motion of each segment, for example, by fixing a certain number of markers on the subject's body. Functional techniques'

formulations make it possible to analyze kinematic deviations and non-standard individuals with deformities. They are very successful at delivering information on the actual DoFs and motion patterns permitted by a particular human joint since they don't call for any a priori definition of the joint center or AoR. Among the several techniques available [11–15], helical axis (HA) theory and symmetrical axis of rotation approach (SARA) have proven to be able to provide quantitative knowledge about joint AoR [16], starting from motion capture data and often by considering custom-made marker protocols.

This study aims to present the design of a HAFO prototype built in additive manufacturing and functionally customized by implementing AoR estimation techniques on a single healthy subject. In particular, the instantaneous helical axis (IHA) and SARA techniques are taken into account. A prototype of the brace is shown, along with a description of the design of the mechanical hinge. The study also presents the results of kinematic studies conducted on the same individual in barefoot condition and while wearing the orthosis, with the purpose to assess the biomechanical effect of the brace on normal motion tasks.

2 Method for in-vivo investigation of joint biomechanics

2.1 Motion capture analysis with rigid shells

Custom-made stiff shells at the foot (FS) and shank (SS) were created and built by fused deposition modeling (FDM) in order to minimize the impact of soft-tissue artifacts on AoR estimation [5]. These shells were employed for the optimal marker location and segment tracking. A healthy subject (woman, 24 years) was recruited. The subject was standing barefoot with the left foot in phenolic foam. The left shank and the dorsal aspect of the foot were captured using a portable 3D optical scanner (EinScan-Pro, Shining 3D) (Fig. 1a), while the plantar aspect of the foot was captured by doing a scan of the foam itself (Fig. 1b). After smoothing process, the skin surfaces from the scan were joined and recreated using a volumetric algorithm in MeshLab once the mesh had been processed. Then, the shells (1.5 mm thickness) were designed directly on top of the scanned surfaces in SolidWorks, by considering the frontal aspect of the shank and the rear-foot and mid-foot anatomy (Fig. 1c). Four areas were also highlighted on each model in order to facilitate the placement of reflective markings over the shells. Moreover, openings for Velcro straps were included in each shell for fastening.

A 3D-printer (UltiMaker S5) based on FDM technology was utilized to create the shells by using PLA (2.85 mm filament, 3D Italy). The SS was oriented vertically, while the FS was orientated with its longitudinal axes parallel to the horizontal plane, to shorten the production time and to reduce the amount of support material. To prevent skin harm, the inside surfaces of the shells were coated with thin, soft cushions. The shells were utilized to collect motion analysis data in order to evaluate the native kinematics of the ankle joint, which was considered as the basis for custom HAFO design.

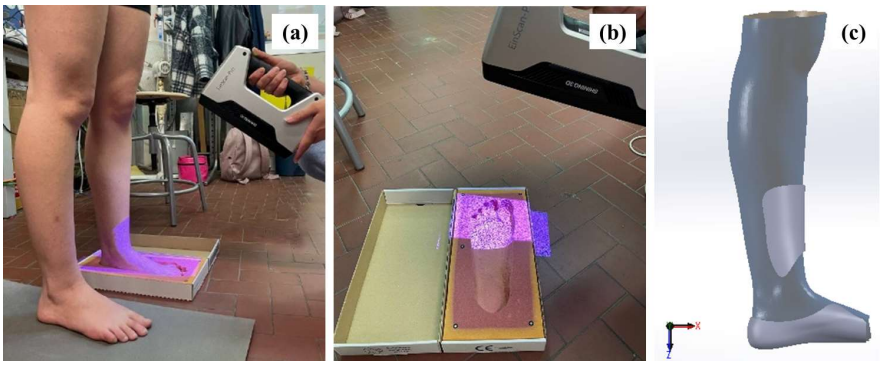

Fig. 1. Rigid shells modeling: (a) shank scan; (b) foot sole scan; (c) 3D reconstruction.

Motion data from the participant was recorded at 100 Hz using a stereo-photogrammetric system (Vicon Motion Capture, UK) with 12 digital cameras and two force plates (AMTI, USA). Motion trials included 5 consecutive level walking repetitions (14 gait cylces) and 7 cycles of active dorsi-plantarflexion performed directly by the subject with her foot lifted from the ground. Both tasks were performed at self-selected, natural-like, speed (walk: 0.97 ± 0.05 m/s; dorsi-plantarflexion = 0.61 cycles/s). For the walking trials, two different marker-sets (14 mm in diameter) were used. Traditional lower limb Plug-in-Gait (PiG) was used to assess ankle angular kinematics and to evaluate spatio-temporal parameters of gait. In addition to that, a custom marker-set [5, 16] was implemented to track SS and FS motion patterns (Fig. 2a-b), in both walking (Fig. 2c) and dorsi-plantarflexion (Fig. 2d) trials to apply IHA and SARA methods.

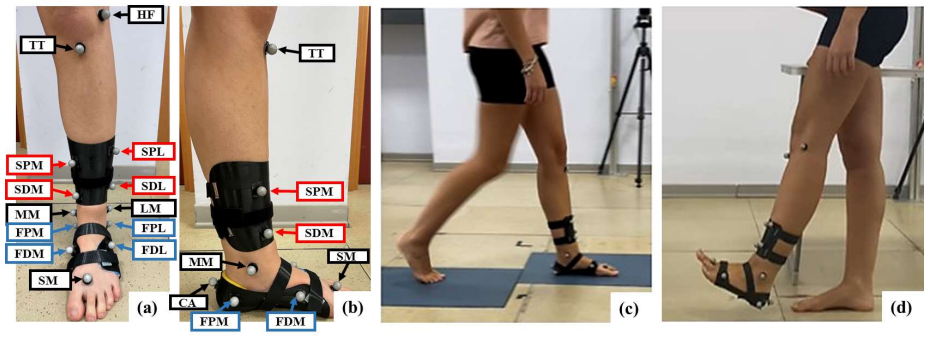

Fig. 2. Motion analyses performed with rigid shells: custom marker-set in front (a) and lateral (b) views; (c) level walking; (d) dorsi-plantarflexion.

A direct comparison with the 3D model of the shank and foot (fitted with the shells, as shown in Fig. 1c) was required to confirm the proper placement of both SS and FS. As the SS does not include any particular bone protrusion or landmark, this technique was necessary whereas the calcaneus and rear-foot provided more reliable references to the FS positioning.

2.2 Algorithms for joint axis estimation

In this section, the methodologies considered for the estimation of the AoR are presented. The two algorithms, implemented in MATLAB code, were mainly selected to allow for a more robust discussion about the accuracy of AoR estimation, given that the identification of the *true* joint AoR would require invasive and/or more expensive techniques.

IHA estimation technique takes into account the helical motion assumption of a screw [17]. This approach calls for the transformation of the global trajectories of the SS and FS markers in the Local Coordinate System (LCS) of the SS. A rigid body fitting procedure based on Singular Value Decomposition (SVD) is then used to solidify FS markers [18]. The direction and the position vector representative of the IHA are calculated using the filtered DoF and their temporal derivatives for each *i*-th time frame. Finally, a cutoff of 0.25 rad/s is fused to filter out time frames that occur when the helical axis could be estimated incorrectly. Given the full representation of the joint kinematics provided by a set of IHAs, a Mean Helical Axis (MHA) can be calculated by a weighted least square algorithm [15, 19, 20].

SARA method utilized in this study takes into account two marker sets that are concurrently moving and is based on the original work of Ehrig et al [21, 22]. A LCS is given to each marker cluster, or segment, in order to perform the algorithm. The estimated AoR is thought to remain stable with regard to the corresponding segment by mathematical formulation, according to SARA. The evaluation of the rotation matrices and translation vectors linked to each segment is done via rigid body transformations, by minimization of an objective function [21, 23]. The location and orientation vectors for each LCS are produced by solving a linear least squares problem, using SVD. Because to the algorithm's inherent time-independence, these parameters are produced as two pairs of constant vectors. An average of them is calculated for each time frame, to estimate the joint AoR.

To compare the two methods, the axes calculated by the SARA and IHA techniques were both represented in the shank anatomical reference system. In addition, the rms distance and orientation between the mean and the instantaneous axis were calculated using the linear (d_{eff}) and angular (χ_{eff}) dispersion parameters for both methods [16].

2.3 Results of AoR estimation in motion trials performed with rigid shells

In average, IHA estimation resulted in d_{eff}=22.3 mm and χ_{eff}=34.9° for walking, and in d_{eff}=14.5 mm and χ_{eff}=30.8° for dorsi-plantarflexion. As expected, SARA provided far more restricted AoR datasets, yielding to d_{eff}=1 mm and χ_{eff}=1.7° for walking, and to d_{eff}=2.2 mm and χ_{eff}=3° for dorsi-plantarflexion. The two algorithms showed similar results for the AoR calculated in active dorsi-plantarflexion tasks. Walking trials, on the other hand, provided two different AoR configurations that significantly limit the possibility to affirm a comparison between the two algorithms tested. In addition, as signaled by the higher dispersion values, IHA-estimated axes resulted always in less robust datasets. On the other hand, SARA algorithm provided the most consistent result for most of the cycles and repetitions considered. The current investigation verified that

the ankle joint's rotational axis (Fig. 3) considerably deviates from the generic, fixed axis used in many commercial braces, that does not match with anatomical or functional criteria specific of the subject [6].

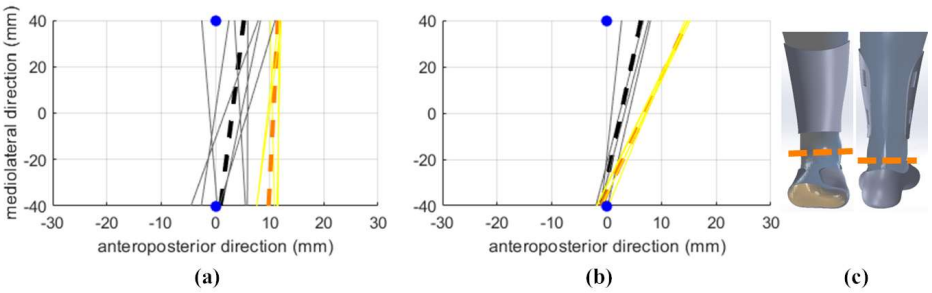

Fig. 3. Ankle joint AoR estimated through SARA algorithm (yellow lines) and IHA (grey lines) for multiple cycles and their respective mean axis (dashed bold lines): (a) level walking task; (b) dorsi-plantarflexion task; (c) hinge axis placement in CAD model of lower limb and shells.

It is evident that walking tasks represent a typical condition in which the orthosis carries out its functionality, however it is likewise predictable that a patient suffering from diseases at the ankle-foot complex could not be able to walk properly. The results of the aforementioned analysis show that dynamic loads at the joint during walking and the movements occurring outside the sagittal plane, affect the robustness and accuracy of AoR estimation, impacting the quality of the result in different ways when considering IHA and SARA algorithms. On the other hand, dorsi-plantarflexion tasks enable a smoother analysis and far more consistent results between the two algorithms. For this reason, the average AoR resulting from that motion task, obtained by considering SARA algorithm, was selected as the reference for the hinge design in the HAFO prototype (Fig. 3b).

3 HAFO design and joint axis customization

In order to link the two shells of the HAFO, a unique mechanical articulation was created. The SS and FS designed for preliminary kinematic estimation have been thickened up to 2.5 mm, in order to provide a more stable support and to be compliant with similar devices from the literature [24, 25]. Moreover, two extensions were added to both shells to accommodate the components of the hinge laterally and medially. As shown in Fig. 4a, a cylindrical part (in green) was fixed to the FS, whereas a second cylindrical component (in blue) was fixed to the SS. A third component (in red) was used to hold externally the hinge in position. The hinge components were located coherently with the positioning of the target AoR estimated by the methodology shown in section 2.3 and oriented to achieve joint flex-extension about the AoR. A cut along the outer cylindrical surface of the green component worked as end-stop for the hinge and allowed for 60° of dorsiflexion and 30° of plantarflexion. Out-of-sagittal plane rotations, namely prono-

supination and abduction-adduction, were restricted as well as the three joint translations, due to the limited dispersion of the dataset resulting from SARA algorithm, that evidenced only 2.2 mm and 3° deviations from the average AoR. Limited variability in the joint AoR was still allowed by elastic deformation of the orthosis and hinge components.

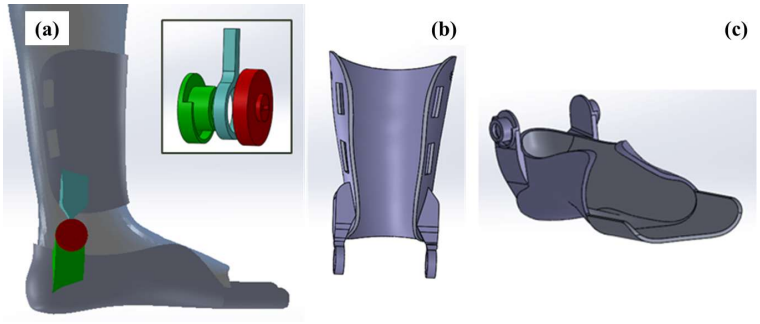

Fig. 4. CAD model of HAFO prototype: (a) details of hinge joint; (b) shank shell; (c) foot shell.

The hinge components were integrated directly in the geometry of the shells (Fig. 4b-c). Therefore, the HAFO shells had to be manufactured specifically. In the final prototype, the SS was 3D-printed along the antero-posterior axis of the shell, in order to achieve high stiffness in the hinge components. The FS was still manufactured by considering its longitudinal axis parallel to the base of support. Similarly to the preliminary shells, openings for Velcro straps and cushions were added to ease the wearability of the device.

4 Kinematic validation

The functionality of the HAFO prototype was evaluated by performing motion analyses with similar approach as shown in section 2.1. A total of 12 gait cycles and 7 dorsi-plantarflexion cycles were performed by the subject after familiarization with the HAFO.

Primarily, the conformity between device's kinematics and the one preliminary identified on the subject had to be verified. For this reason, dorsi-plantarflexion trials was simulated by an operator maneuvering the shells by choosing the marker-set shown in Fig. 2a-b. The AoR emerging from passive dorsi-plantarflexion (green line, Fig. 5) is consistent with the lateral (LJ) and medial (MJ) placement of the hinge components, that were tracked with reflective markers (red line, Fig. 5). The differences between the two axes are probably due to the joint translations allowed by joint backlash and elastic deformations. The dorsi-plantarflexion axis is also coherent with the theoretical axis (blue line, Fig. 5) selected for HAFO design (Fig. 3), apart from slight differences in the transverse plane. The latter might be related to alterations in markers positioning that affect the comparison between trials conducted with and without the orthosis. To avoid this issue, in future studies the orthosis could be manufactured directly by

properly connecting a hinge to the same shank and foot shells that were used to gather kinematic trials.

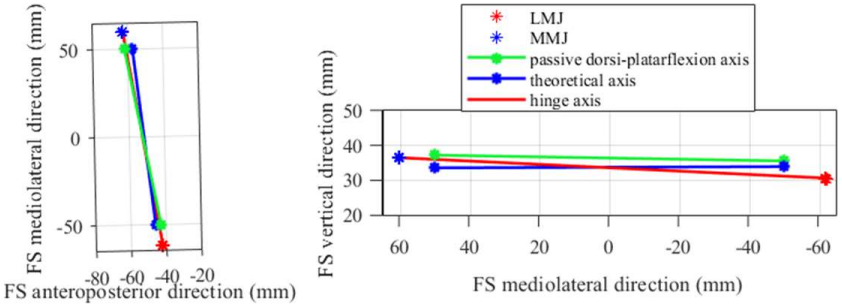

Fig. 5. Joint AoR estimated with SARA in trials performed with the HAFO.

Secondly, the effect of the HAFO prototype on subject's kinematics was evaluated. To this purpose, gait trials were performed and processed by choosing PiG protocol. The latter was considered to assess changes in angular kinematics and spatio-temporal parameters due to the orthosis. Because the malleoli were obscured by the foot shell, the markers had to be positioned 1 cm above and 1 cm behind the actual anatomical landmarks. Figure 6a shows the results of left ankle angular kinematics in gait trials performed by wearing the HAFO (Fig. 6b).

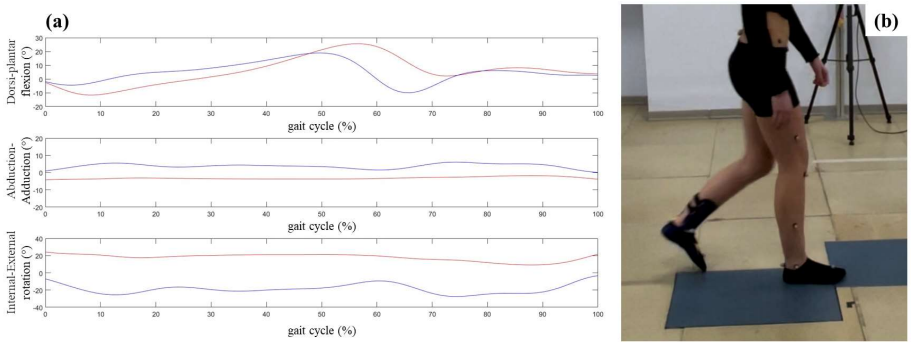

Fig. 6. (a) Angular kinematics data for ankle joint estimated during gait trials (b).

Flex-extension in sagittal plane results fundamentally unaltered, except for increased plantarflexion around 60% of the gait cycle, whereas motion in other planes is significantly restricted as expected. A bias error was observed, probably due to slightly different positioning in markers between the trials conducted in barefoot and HAFO conditions. However, this aspect might be investigated in the future to rule out the possibility of any undesired prono-supination and adduction-abduction angles forced by the orthosis on the ankle joint.

Figure 7 shows spatio-temporal parameters resulting from the analysis on multiple gait repetitions, averaged by considering up to 3 full gait cycles for each walking trial.

By comparing swing and stance times obtained in both conditions, it is quite evident that the orthosis does not significantly alter the balance between the two phases of gait. The same behavior has been observed for both limbs, although the results are shown only for left leg for sake of conciseness. Therefore, it can be concluded that the device does not negatively affect the symmetry of steps. At the same time, stride length is reduced in all trials and stride time results increased. This result, that was expected since visual inspection of the subject in the laboratory, can be mainly related to the limited perception of the subject at the foot contact with the floor, which affects stability and comfort in wearing the device, and to the stiffness of the device that still restricts ankle motion occurring within the sagittal plane, due to hinge end-stops, and in transverse and coronal planes.

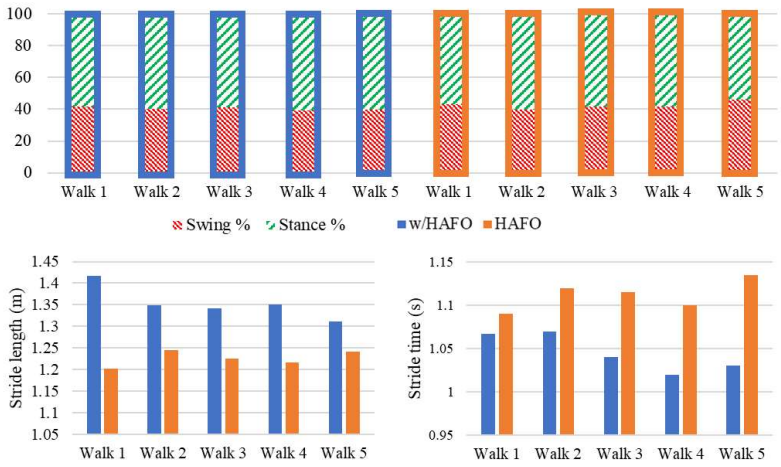

Fig. 7. Spatio-temporal parameters for gait analyses in barefoot condition and with the HAFO. Swing and stance time percentages are shown only for the left leg.

5 Conclusion

An approach for creating a unique hinged ankle-foot orthosis has been put forth in this study, with a particular emphasis on the quantitative analysis of the natural joint kinematics for motion tasks carried out by a single healthy subject. The results of this work show that the device is able to restrict motion in coronal and transverse planes without negatively altering dorsi-plantarflexion in the sagittal plane. However, the study shows some limitations that will be discussed briefly and could be objective of future work.

Differences were observed in the kinematic results from walking and dorsi-plantarflexion trials. However, the two algorithms for AoR estimation (SARA and IHA) showed inconsistent results, in particular for gait trials. The effect of dynamic load occurring during walking should be verified to assess the robustness of each algorithm.

The study considered only a single, healthy subject and represents a pilot experiment conducted to evaluate the feasibility of the methodology proposed. However, that

should be verified on a larger sample of subjects, which could include patients with diseases at the ankle-foot complex. Especially for unhealthy subjects, the choice of a representative motion task for kinematic identification is critical. In that case, an artificial increase or reduction of range of motions could be necessary to fit a specific therapeutic problem. Of course, this aspect should be verified by experimentation and its feasibility confirmed in clinics.

The variability in AoR datasets obtained from dorsi-plantarflexion trials was very limited. On the other hand, walking trials resulted in far more disperse datasets, especially considering the IHA methodology. If walking trials could be considered representative for HAFO design, a floating-axis hinge would be necessary to accommodate this behavior.

The prototype shown in this paper has limited encumbrance around shank and foot shells, but it is quite bulky in the area of hinge components that protrude laterally for few centimeters. For this reason, different geometries for HAFO shells and hinge components should be studied, to improve ergonomics and wearability of the device inside a common or adapted shoe.

References

1. Kluding, P.M., Dunning, K., O'Dell, M.W., Wu, S.S., Ginosian, J., Feld, J., McBride, K.: Foot Drop Stimulation Versus Ankle Foot Orthosis After Stroke: 30-Week Outcomes. Stroke. 44(6), 1660–1669 (2013). https://doi.org/10.1161/STROKEAHA.111.000334.
2. Ries, A.J., Schwartz, M.H.: Ground reaction and solid ankle-foot orthoses are equivalent for the correction of crouch gait in children with cerebral palsy. Dev Med Child Neurol. 61(2), 219–225 (2019). https://doi.org/10.1111/dmcn.13999.
3. Nolan, K.J., Savalia, K.K., Yarossi, M., Elovic, E.P.: Evaluation of a dynamic ankle foot orthosis in hemiplegic gait: A case report. NRE. 27(4), 343–350 (2010). https://doi.org/10.3233/NRE-2010-0618.
4. Del Bianco, J., Fatone, S.: Comparison of Silicone and Posterior Leaf Spring Ankle-Foot Orthoses in a Subject With Charcot-Marie-Tooth Disorder. JPO Journal of Prosthetics and Orthotics. 20(4), 155–162 (2008). https://doi.org/10.1097/JPO.0b013e31818addbd.
5. Ferraresi, C., De Benedictis, C., Bono, L., Del Gaudio, F., Ferrara, L., Masiello, F., Franco, W., Maffiodo, D., Leardini, A.: A methodology for the customization of hinged ankle-foot orthoses based on in vivo helical axis calculation with 3D printed rigid shells. Proc Inst Mech Eng H. 235(4), 367–377 (2021). https://doi.org/10.1177/0954411920981543.
6. Leardini, A., Aquila, A., Caravaggi, P., Ferraresi, C., Giannini, S.: Multi-segment foot mobility in a hinged ankle-foot orthosis: the effect of rotation axis position. Gait & Posture. 40, 274–277 (2014). https://doi.org/10.1016/j.gaitpost.2014.03.188.
7. Seidel, G.K., Marchinda, D.M., Dijkers, M., Soutas-Little, R.W.: Hip joint center location from palpable bony landmarks—A cadaver study. Journal of Biomechanics. 28(8), 995–998 (1995). https://doi.org/10.1016/0021-9290(94)00149-X.
8. Kadaba, M.P., Ramakrishnan, H.K., Wootten, M.E.: Measurement of lower extremity kinematics during level walking. J. Orthop. Res. 8(3), 383–392 (1990). https://doi.org/10.1002/jor.1100080310.
9. Ehrig, R.M., Heller, M.O.: On intrinsic equivalences of the finite helical axis, the instantaneous helical axis, and the SARA approach. A mathematical perspective. Journal of Biomechanics. 84, 4–10 (2019). https://doi.org/10.1016/j.jbiomech.2018.12.034.

10. Leardini, A., O'Connor, J.J., Catani, F., Giannini, S.: Kinematics of the human ankle complex in passive flexion; a single degree of freedom system. Journal of Biomechanics. 32(2), 111–118 (1999). https://doi.org/10.1016/S0021-9290(98)00157-2.
11. MacWilliams, B.A.: A comparison of four functional methods to determine centers and axes of rotations. Gait & Posture. 28(4), 673–679 (2008). https://doi.org/10.1016/j.gaitpost.2008.05.010.
12. Asadi Nikooyan, A., van der Helm, F.C.T., Westerhoff, P., Graichen, F., Bergmann, G., (Dirkjan) Veeger, H.E.J.: Comparison of Two Methods for In Vivo Estimation of the Glenohumeral Joint Rotation Center (GH-JRC) of the Patients with Shoulder Hemiarthroplasty. PLoS ONE. 6(3), e18488 (2011). https://doi.org/10.1371/journal.pone.0018488.
13. Monnet, T., Desailly, E., Begon, M., Vallée, C., Lacouture, P.: Comparison of the SCoRE and HA methods for locating in vivo the glenohumeral joint centre. Journal of Biomechanics. 40(15), 3487–3492 (2007). https://doi.org/10.1016/j.jbiomech.2007.05.030.
14. De Rosario, H., Page, Á., Mata, V.: Point of optimal kinematic error: Improvement of the instantaneous helical pivot method for locating centers of rotation. Journal of Biomechanics. 47(7), 1742–1747 (2014). https://doi.org/10.1016/j.jbiomech.2014.02.003.
15. Ferraresi, C., De Benedictis, C., Franco, W., Maffiodo, D., Leardini, A.: In-vivo analysis of ankle joint movement for patient-specific kinematic characterization. Proc Inst Mech Eng H. 231(9), 831–838 (2017). https://doi.org/10.1177/0954411917709492.
16. De Benedictis, C.: Comparison between Helical Axis and SARA Approaches for the Estimation of Functional Joint Axes on Multi-Body Modeling Data. Applied Sciences. 12(3), 1274 (2022). https://doi.org/10.3390/app12031274.
17. Woltring, H.J., Huiskes, R., de Lange, A., Veldpaus, F.E.: Finite centroid and helical axis estimation from noisy landmark measurements in the study of human joint kinematics. Journal of Biomechanics. 18(5), 379–389 (1985). https://doi.org/10.1016/0021-9290(85)90293-3.
18. Cappello, A., La Palombara, P.F., Leardini, A.: Optimization and smoothing techniques in movement analysis. International Journal of Bio-Medical Computing. 41(3), 137–151 (1996). https://doi.org/10.1016/0020-7101(96)01167-1.
19. Stokdijk, M., Meskers, C.G.M., Veeger, H.E.J., de Boer, Y.A., Rozing, P.M.: Determination of the optimal elbow axis for evaluation of placement of prostheses. Clinical Biomechanics. 14(3), 177–184 (1999). https://doi.org/10.1016/S0268-0033(98)00057-6.
20. Burton, K.: Biomechanics of human movement: applications in rehabilitation, sports and ergonomics. Clinical Biomechanics. 7(4), 251 (1992). https://doi.org/10.1016/0268-0033(92)90010-2.
21. Ehrig, R.M., Taylor, W.R., Duda, G.N., Heller, M.O.: A survey of formal methods for determining the centre of rotation of ball joints. Journal of Biomechanics. 39(15), 2798–2809 (2006). https://doi.org/10.1016/j.jbiomech.2005.10.002.
22. Ehrig, R.M., Taylor, W.R., Duda, G.N., Heller, M.O.: A survey of formal methods for determining functional joint axes. Journal of Biomechanics. 40(10), 2150–2157 (2007). https://doi.org/10.1016/j.jbiomech.2006.10.026.
23. Reichl, I., Auzinger, W.: Identifying Tibio-Femoral Joint Kinematics: Individual Adjustment versus Numerical Robustness. IFAC Proceedings Volumes. 45(2), 819–824 (2012). https://doi.org/10.3182/20120215-3-AT-3016.00145.
24. Dal Maso, A., Cosmi, F.: 3D-printed ankle-foot orthosis: a design method. Materials Today: Proceedings. 12, 252–261 (2019). https://doi.org/10.1016/j.matpr.2019.03.122.
25. Patel, P., Gohil, P.: Custom orthotics development process based on additive manufacturing. Materials Today: Proceedings. 59, A52–A63 (2022). https://doi.org/10.1016/j.matpr.2022.04.858.